


ORIGINAL RESEARCH

The first description of a hormone-sensitive lipase from a basidiomycete: Structural insights and biochemical characterization revealed *Bjerkandera adusta* BaEstB as a novel esterase

María del Rayo Sánchez-Carbente¹ | Ramón Alberto Batista-García² |
Ayixón Sánchez-Reyes^{1,2} | Angela Escudero-García¹ | Catalina Morales-Herrera¹ |
Laura I. Cuervo-Soto^{1,3} | Leidys French-Pacheco⁴ | Arline Fernández-Silva⁴ |
Carlos Amero⁴ | Edmundo Castillo⁵ | Jorge Luis Folch-Mallol¹ 

¹Centro de Investigación en Biotecnología, Universidad Autónoma del Estado de Morelos, Cuernavaca, Morelos, Mexico

²Centro de Investigación en Dinámica Celular, Instituto de Investigación en Ciencias Básicas y Aplicadas, Universidad Autónoma del Estado de Morelos, Cuernavaca, Morelos, Mexico

³Departamento de Biología, Facultad de Ciencias, Universidad Antonio Nariño, Bogota, Colombia

⁴Centro de Investigaciones Químicas, Instituto de Ciencias Básicas y Aplicadas, Universidad Autónoma del Estado de Morelos, Cuernavaca, Morelos, Mexico

⁵Instituto de Biotecnología, Universidad Nacional Autónoma de México, Cuernavaca, Morelos, Mexico

Correspondence

Jorge Luis Folch-Mallol, Centro de Investigación en Biotecnología, Universidad Autónoma del Estado de Morelos, Cuernavaca, Mexico.
Email: jordi@uaem.mx

Funding information

This work was supported by grants from the National Council for Science and Technology (CONACyT)-Mexico: Project CB-153789 and partly by PRODEP-SEP Project UAEMOR-PTC-333 and Project PAPIIT-UNAM IN209016. RABG, ASR, AEG, CMH, LICs, LFP, and AFS received a scholarship from the CONACyT, Mexico

Abstract

The heterologous expression and characterization of a Hormone-Sensitive Lipases (HSL) esterase (*BaEstB*) from the Basidiomycete fungus *Bjerkandera adusta* is reported for the first time. According to structural analysis, amino acid similarities and conservation of particular motifs, it was established that this enzyme belongs to the (HSL) family. The cDNA sequence consisted of 969 nucleotides, while the gene comprised 1133, including three introns of 57, 50, and 57 nucleotides. Through three-dimensional modeling and phylogenetic analysis, we conclude that *BaEstB* is an ortholog of the previously described *RmEstB*-HSL from the phylogenetically distant fungus *Rhizomucor miehei*. The purified *BaEstB* was characterized in terms of its specificity for the hydrolysis of different acyl substrates confirming its low lipolytic activity and a noticeable esterase activity. The biochemical characterization of *BaEstB*, the DLS analysis and the kinetic parameters determination revealed this enzyme as a true esterase, preferentially found in a dimeric state, displaying activity under alkaline conditions and relative low temperature (pH = 10, 20°C). Our data suggest that *BaEstB* is more active on substrates with short acyl chains and bulky aromatic moieties. Phylogenetic data allow us to suggest that a number of fungal hypothetical proteins could belong to the HSL family.

KEYWORDS

Bjerkandera adusta, ergosterol esters, esterase, Hormone-Sensitive Lipase

This is an open access article under the terms of the Creative Commons Attribution License, which permits use, distribution and reproduction in any medium, provided the original work is properly cited.

© 2017 The Authors. *MicrobiologyOpen* published by John Wiley & Sons Ltd.

1 | INTRODUCTION

Esterases (carboxylic ester hydrolases, EC 3.1.1) including lipases (triacylglycerol hydrolases, EC 3.1.1.3.) are important biocatalysts that mediate stereospecific hydrolysis, transesterification and a variety of primary and secondary alcohols (Akoh, Lee, Liaw, Huang, & Shaw, 2004; Lopes, Fraga, Fleuri, & Macedo, 2011). Due to their particular properties such as broad substrate specificity, high chemo-, regio- and stereoselectivity and generally with no requirement for cofactors, these enzymes have a wide variety of industrial uses such as the production of detergents, pharmaceuticals, cosmetics, and paper as well as in biodiesel industry among others (Andualema & Gessesse, 2012; Bornscheuer, 2002; Carrière et al., 1998; Chahinian & Sarda, 2009). While lipases act on water-insoluble substrates, such as long-chain triglycerides, esterases hydrolyze preferentially 'simple' esters and usually only triglycerides bearing short-chain fatty acids (<C₁₀) (Jaeger, Dijkstra, & Reetz, 1999). Most of lipases can also be distinguished from esterases by the phenomenon of interfacial activation, where the enzymes are active at the interface between their hydrophobic lipid substrate and the hydrophilic medium (oil-water interface) (Fojan, Jonson, Petersen, & Petersen, 2000).

Esterases and lipases have been isolated from microorganisms, plants, animals, and metagenomes (Fojan et al., 2000; Gopinath, Anbu, LakshmiPriya, & Hilda, 2013). They have also been produced in heterologous hosts upon bioinformatics screening of public databases of genomes (Barriuso, Prieto, & Martínez, 2013). There is still interest in the characterization of microbial lipolytic enzymes and esterases because of their high production yields and the easy genetic manipulation of the microorganisms compared with other organisms. Both enzymes share the α/β fold in their structure and most of them present the consensus sequence GX SXG as a signature motif. According to amino acid similarities and conservation of particular motifs, lipolytic enzymes (including esterases) are classified into C, H, X, and L blocks (Lenfant et al., 2013).

Block H includes Hormone-Sensitive Lipases (HSL), where the majority of the enzymes resulted to be esterases (Ali, Verger, & Abousalham, 2012; Huang et al., 2016; Li et al., 2015). In mammals, HSL have been proposed as esterases that hydrolyze diacylglycerol for the generation of ATP and cholesteryl esters precursors to deliver cholesterol for the synthesis of steroid hormones (Kraemer, 2007). In fungi, ergosterol is used instead of cholesterol to maintain fluidity, permeability and integrity of the plasma membrane and adequate function of membrane-bound proteins (Holick, 2003; Sun, Gao, Ling, & Lou, 2005). Ergosterol esters are found in lipid particles in the cytoplasm and when unesterified may be used as a source for ergosterol in membrane synthesis (Shobayashi et al., 2005; Zweytick, Athenstaedt, & Daum, 2000).

Bacterial lipolytic enzymes are classified in eight families, where proteins with high similarity to mammalian HSL belong to family IV (Arpigny & Jaeger, 1999). Based on massive sequence alignment and different conserved motifs, two subfamilies of bacterial HSL have been proposed, the GTSAG motif subfamily and the GDSAG motif subfamily, where the labeled amino acids are defined as arbitrary residues in the pentapeptide conserved motif GX SXG (Jeon et al., 2012; Li et al., 2014).

Lipolytic enzymes from fungi have been extensively characterized from *Candida antarctica*, *C. rugosa*, and from filamentous fungi as *Aspergillus niger*, *Rhizopus oryzae*, *Penicillium camembertii* among others, that have been commercialized and used in dairy, oil, and fat industries (Anobom et al., 2014; Borrelli & Trono, 2015; Houde, Kademi, & Leblanc, 2004). However, only two fungal lipolytic enzymes from the HSL family (*RmEstA* and *RmEstB*) have been studied (*Rm*: *Rhizomucor miehei*, Est: Esterase). Both of them were identified from the mucoral thermophilic fungus *R. miehei*. Interestingly, *RmEstA* and *RmEstB* exhibit distinct substrate specificities: *RmEstA* shows high activity toward long-chain esters, whereas *RmEstB* favors hydrolysis of short-chain esters (Liu et al., 2013; Yan et al., 2014; Yang, Qin, Duan, Yan, & Jiang, 2015). In spite of these reports, there is still a lack of information of lipolytic enzymes from the HSL family in fungi and their role is uncertain.

Bjerkandera adusta is a "white-rot" Basidiomycete well known for its high ligninolytic activities (Romero, Speranza, García-Guinea, Martínez, & Martínez, 2007; Wang, Vazquez-Duhalt, & Pickard, 2003), which are attractive to biorefinery and bioremediation fields. Few reports have described its extracellular enzymatic activities from crude extracts (Bancerz & Ginalska, 2007; Quiroz-Castañeda, Pérez-Mejía, Martínez-Anaya, Acosta-Urdapilleta, & Folch-Mallol, 2011; Quiroz-Castañeda et al., 2009). Only two *B. adusta*'s genes from strain UAMH-8258 have been cloned and overexpressed in heterologous systems and their proteins characterized: a loosenin (an expansin-like protein) (Quiroz-Castañeda, Martínez-Anaya, Cuervo-Soto, Segovia, & Folch-Mallol, 2011) and a carbohydrate esterase (Cuervo-Soto et al., 2015). Interestingly, a report in 2005 showed that *B. adusta* R59 degrades highly recalcitrant xenobiotics such as the anthraquinonic antibiotic daunomycin and other humic acids. Among the enzymatic activities secreted by the fungus to degrade the xenobiotics were lacases, peroxidases, cellulases, hemicellulases, and lipolytic enzymes. Moreover, lipolytic activity was stimulated in the presence of humic acids (Belcarz, Ginalska, & Kornilowicz-Kowalska, 2005). However, the study did not show data of purified enzymes.

In this work, we report the characterization of the first HSL esterase reported from a Basidiomycete (*BaEstB*). The cDNA was obtained from a *B. adusta* library grown on crude oil. Blastp results showed high similarity with esterase family IV that includes HSL members. Classification within the HSL family was confirmed through phylogenetic analysis and homology modeling of *BaEstB*. The esterase activity was confirmed by the preference of the enzyme for shorter chain substrates and the lack of activity on a rhodamine triglyceride assay.

2 | MATERIALS AND METHODS

2.1 | *BaEstB* modeling, structural alignment, three-dimensional superposition and structure-based and sequence-based phylogenies

Upon PSI-BLAST (Position-Specific Iterated) analysis of 768 sequenced clones from a cDNA library from *B. adusta*, we identified a sequence with homology to the α/β hydrolase Esterase/Lipase

superfamily. The Open Reading Frame (ORF) in this sequence was named as *BaEstB* (GenBank accession number KX580963). The complete amino acid sequence of the *BaEstB* was submitted to the I-TASSER server (Roy, Kucukural, & Zhang, 2010; Yang, Qin, et al., 2015; Yang, Yan, et al., 2015; Zhang, 2008) without constraints in order to get a three-dimensional model. A second modeling round was performed using PDB (Protein Data Bank) 4WY8 and 4ZRS as templates, since these PDBs were the best templates found during the first modeling round. Structural alignments and three-dimensional superpositions were obtained considering the PDBs identified by I-TASSER as close structural neighbors in order to identify the cap and catalytic domains, the catalytic triad, the conserved motifs, and other residues involved in the catalysis of *BaEstB*. The model visualization and structural alignment, including the Root Mean Square Deviation (RMSD) values, were obtained in Visual Molecular Dynamic program (VMD) (Humphrey, Dalke, & Schulten, 1996).

A structure-based phylogenetic tree according with the RMSD derived from *BaEstB*'s structural comparison with its closest structural analogs was prepared in VMD and visualized in Phylogeny.fr server (<http://www.phylogeny.fr/>). A second phylogenetic tree (amino acid sequence-based reconstruction) was obtained on line in the same server in order to describe the relationships of *BaEstB* with related sequences obtained from the Blast results. Phylogeny.fr considers various bioinformatics algorithms to construct a robust phylogenetic tree from a set of sequences (Dereeper, Audic, Claverie, & Blanc, 2010; Dereeper et al., 2008); for the generation of phylogenetic trees, MUSCLE was used for the multiple alignments, Gblocks for the automatic alignment curation (in order to eliminate poorly aligned positions, not allowing smaller final blocks and less strict flanking positions), PhyML, for tree building and TreeDyn for tree drawing (Dereeper et al., 2008). The Maximum Likelihood method was used to estimate the phylogenetic tree; the branch support was assessed using the ALTr algorithm and the Jones-Thornton-Taylor (JTT) model was used to estimate distances for amino acids (Dereeper et al., 2008). The parameters used during the MUSCLE alignment were those recommended by the Phylogeny.fr platform (custom mode with 16 as the maximum number of iterations). A lipase from *Candida cylindracea* (gi: 1325988) was used as an outgroup.

2.2 | Cloning of *BaEstB*

The coding sequence of the *BaEstB* was amplified using primers Forw*BaEstB* (5'gaattcatggaatctatccgtctgctc3') and Rev*BaEstB* (5'tctagaccctattccgctgctgta3') with cutting sites underlined for *EcoRI* and *XbaI*, respectively, which allowed the subcloning into the expression vector (pPICZαA); the two cytosines in bold were added to put the sequence in frame with the myc- and poly-His tags. The PCR conditions were as follows: 95°C 5 min (one cycle); 95°C 45 s, 55°C 60 s and 72°C 2 min (30 cycles) and a final extension step of 72°C 7 min (one cycle), on a thermocycler (Axigen-Maxigene) and the amplification was carried out with *Pfu* DNA polymerase (Jena Biosciences). The amplified product was purified with the Column DNA Gel Extraction

Spin Kit (Thermo Scientific), ligated into vector pJET (pJET-*BaEstB*) and transformed into *E. coli* DH5α electrocompetent cells for subsequent sequencing.

The genomic sequence of *BaEstB* was obtained using the Genome Walker Kit (Clontech) following the manufacturer's instructions using oligonucleotides pDNRIlib Fwd: 5' ACCATGGAATCTATCCGTCT 3' and pDNRIlib Rev: 5' AGAAAATGTCATTACGGTGG 3'. The PCR conditions were as follows: 95°C-5 min (one cycle), 95°C 1 min; 57°C 30 s; 73°C 2 min (30 cycles); and a final extension step of 73°C for 5 min, using the same apparatus and enzyme as described above. The amplified fragments were purified as described above for sequencing.

2.3 | Expression of *BaEstB* in *Pichia pastoris* X-33 and enzyme purification

pJET-*BaEstB* was digested with *EcoRI* and *XbaI*, and the released *BaEstB* cDNA fragment was inserted into pPICZαA (Invitrogen, USA) digested with the same enzymes. This construct was designated as pPICZαA/*BaEstB* and was transformed into *E. coli* DH5α. Restriction digestion and DNA sequencing verified the identity of the insert. This construction was linearized with *SacI*, and *P. pastoris* X-33 cells were transformed by electroporation for 5 ms at 2,000 volts employing an Eporator apparatus (Eppendorf). Positive transformants were selected for their ability to grow on Yeast-Peptone-Dextrose (YPD) plates containing zeocin at a final concentration of 100 µg/ml. *P. pastoris* X-33 transformed with the empty vector pPICZαA was used as a negative control. Integration of the *BaEstB* gene into the *P. pastoris* X-33 genome was confirmed by colony PCR analysis using 5' and 3' AOX1 primers, following instructions of Easy Select *Pichia* Expression Kit (Life Technologies Invitrogen).

Positive transformants were grown in parallel on Minimal Dextrose (MD), and Minimal Methanol (MM) medium plates at 28°C for 48 hr to distinguish between Mut+ (Methanol utilization plus) and Muts (Methanol utilization slow) phenotypes. Five Mut+ colonies were selected. Strains wild type *P. pastoris* X-33, *P. pastoris* X-33 transformed with the empty vector (controls) and Mut+ transformed colonies designed as *BaEstB*-1-5 were inoculated into 15 ml Buffered Complex Medium containing Glycerol (BMGY) in 50 ml flasks and grown at 28°C on a rotary incubator (200–250 rpm) until the OD₍₆₀₀₎ reached 2–6 (16–18 hr). Cells were harvested by centrifugation at 1,500g for 5 min and resuspended in 50 ml Buffered Complex Medium containing Methanol (BMMY) medium in 250 ml flasks at the same temperature and rpm. *BaEstB* expression was induced adding methanol to a final concentration of 0.5% at 24 hr intervals during 4 days. Every day, 5 ml of culture was taken for monitoring esterase activity.

BaEstB was purified from a 96-hr culture supernatant using Nickel affinity chromatography. Briefly, the supernatant was recovered by centrifugation at 1,500g for 10 min and concentrated in a 30 kDa cut-off amicon (GE healthcare). This concentrated preparation was loaded into the Ni-column and eluted with a Tris-HCl 10 mmol/L pH 7.5 and 0.2 mol/L imidazol solution. The purified enzyme was dialyzed and the protein was stored at 4°C until further use.

2.4 | SDS-PAGE and zymogram

Proteins from the crude extracts and from various purification steps were analyzed by sodium dodecyl sulphate polyacrylamide gel electrophoresis (SDS-PAGE) according to the method of Laemmli (1970) using 4.5% stacking gel and 12.0% separating gel. The protein bands were stained with Coomassie brilliant blue R-250. Page Ruler plus was used as molecular weight marker (ThermoScientific).

Esterase activity was assayed and visualized on zymograms, using 12.5% polyacrylamide gels (PAGE). Esterase activity staining was performed as described by Karpushova, Brümmer, Barth, Lange, & Schmid (2005). The gels were finally incubated for 5 min at room temperature in developing solution consisting of 3 mmol/L 2-naphthyl acetate, 1 mmol/L Fast Garnet TR (Sigma) and 100 mmol/L sodium phosphate buffer, pH 7.5. The positive esterase activity was detected by the appearance of orange-colored bands in the gels.

2.5 | Esterase activity and substrate specificity determinations

Routinely, esterase activity was measured using 2-naphthyl acetate as substrate (Soberanes Céspedes, Cruz, Vargas, & Vázquez, 2012). A 2-naphthyl acetate stock solution (54 mmol/L, solution 1) was prepared in acetone. Solution 2 for substrate preparation was prepared as follows: 10 mg of Fast Garnet GBC sulfate salt was dissolved in 100 μ l of 50 mmol/L potassium phosphate buffer (pH 7.01) and 0.1% Triton X-100. Finally, a mixture of 10:0.01:0.05 (v/v/v) of potassium phosphate buffer (pH 7.01) 0.1% Triton X-100/Solution 2/Solution 1, respectively was prepared. Briefly, 10 μ l of diluted (1/1,000) pure esterase (1.3 mg of protein/ml) was added to the substrate solution (190 μ l) plus 100 μ l of 10 mmol/L Tris-HCl buffer pH 7.0. The released 2-naphthol was quantified by measuring the absorbance at 538 nm during 30 min. One unit of esterase activity is defined as the amount of enzyme releasing 1 μ mol of 2-naphthol per minute. The used molar absorption coefficient of 2-naphthol was 23,598 $M^{-1} cm^{-1}$.

The specificity of BaEstB for the length of acyl chain was analyzed using *p*-nitrophenyl acetate (pNPA, C₂), *p*-nitrophenyl butyrate (pNPB, C₄), *p*-nitrophenyl decanoate (pNPD, C₁₀), and *p*-nitrophenyl palmitate (pNPP, C₁₆) as described previously (Selvin, Kennedy, Lejon, Kiran, & Dobson, 2012; Yan et al., 2014). One unit of esterase activity is defined as the amount of enzyme releasing 1 μ mol of *p*-nitrophenol (pNP) per minute. The used molar absorption coefficient of pNP at 410 nm was 17,800 $M^{-1} cm^{-1}$.

The rhodamine B assay, specific for lipases, was conducted according to previous reports (Kouker & Jaeger, 1987). A stock solution with 2.5% (w/v) of olive oil was prepared and autoclaved. Rhodamine B (1 mg/ml) was dissolved in distilled water and filter sterilized (MILLEX® GV 0.2 μ m). A solution containing 0.8% agar in buffer 10 mmol/L Tris-HCl pH 7 was autoclaved and after cooling down to 60°C, 31.25 ml of the olive oil solution and 10 ml of the rhodamine B solution were added per L. This was poured in Petri dishes and when solidified, small wells were carved, filled with the different samples and incubated at 30°C for 16 hr, when the appearance of a fluorescent

halo was detected under UV light (350 nm) in the positive control sample (a *Candida cylindracea* lipase, Sigma L1754).

The biochemical characterization of BaEstB was performed using 2-naphthyl acetate as substrate. All measurements were performed in triplicate.

2.6 | Optimum temperature and stability of BaEstB

Optimum temperature for the enzyme was investigated by measuring the esterase activity at different temperatures (10–60°C) with increments of 10°C. The thermal stability of the esterase was determined by measuring the residual activity of enzyme after a 60-min preincubation employing the aforementioned temperature range with same increments. Specific activities were determined under the same condition mentioned above and using 2-naphthyl acetate as substrate. All measurements were performed in triplicate.

2.7 | pH optimum and pH stability of BaEstB

Optimum pH of the enzyme was determined by varying the pH of the assay reaction mixture using the following buffers: 10 mmol/L Tris-HCl (pH 3.0–7.0) or 10 mmol/L carbonate-bicarbonate (pH 8.0–10.0). The stability of the esterase was determined after preincubating the enzyme in different buffer solutions (pH 3.0–10.0) for 60 min. The residual enzyme activity was then determined under the standard assay conditions. All measurements were performed in triplicate.

2.8 | Kinetic parameters via isothermal titration calorimetry (ITC)

ITC experiments were performed on a Malvern ITC200 instrument by titrating 2-naphthyl acetate into the enzyme suspension within the sample cell. Each single-injection consisted in 38 μ l of 2-naphthyl acetate (170 μ mol/L) and 37 μ l of purified BaEstB. All measurements were performed under the following conditions: temperature 30°C, stirring speed of 750 rpm, reference power of 8 μ cal/s, and 90 min allowing the heat signal return to the baseline. The data were analyzed using Origin 7.0v software for *k*_{cat}, *K*_m, and ΔH determinations.

2.9 | Effect of metal ions, NaCl, solvents, detergents, and EDTA on BaEstB activity

In all the experiments described below, the specific activities were determined using 10 μ l of diluted (1/1,000) pure enzyme (10.08 mg of protein/ml), 2-naphthyl acetate as substrate and 10 mmol/L Tris-HCl buffer (pH 7.0). All measurements were performed in triplicate.

2.10 | Effect of metal ion on BaEstB activity

The effect of several metal ions (Ba²⁺, Mg²⁺, Fe²⁺, Co²⁺, Ni²⁺, Mn²⁺, Zn²⁺, Cu²⁺, Ca²⁺, Ag²⁺, K⁺, Li⁺, Al³⁺) on the BaEstB activity was evaluated in the presence of 10 mmol/L of each metal ion and pH 7. Additionally, the BaEstB stability was determined incubating the enzyme for 1 h at

30°C in Tris-HCl buffer pH 7 in presence of the metal ions. The specific activity was measured and the residual activity was calculated.

2.11 | Effect of NaCl on *BaEstB* activity

BaEstB activity was determined in different salinity conditions. Specific activity was measured by incubating the *BaEstB* in Tris-HCl buffer at 30°C with the addition of NaCl to final concentrations of 0.1, 0.25, 0.5, 1.0, and 2.0 mol/L in the reaction mixtures. The halostability (residual activity expressed in percentage) was also evaluated by incubating the *BaEstB* 1 hr at 30°C in Tris-HCl buffer in presence of 0.1, 0.25, 0.5, 1.0, and 2.0 mol/L NaCl.

2.12 | Effect of solvents on *BaEstB* activity

Specific activity *BaEstB* in the presence of different solvents (30% v/v ethanol, methanol, acetone, isopropanol, 1-butanol, chloroform, hexane, and DMSO) (Selvin et al., 2012) was measured by incubating *BaEstB* in Tris-HCl buffer at 30°C with the addition of the solvents in the reaction mixture.

2.13 | Effect of detergents and EDTA on *BaEstB* activity

The effect of several detergents (Tween 20, Tween 80, SDS, Triton X-100, and CTAB) and EDTA on the *BaEstB* activity was evaluated. Residual activity, expressed in percentage, was calculated by incubating the *BaEstB* in Tris-HCl buffer for 1 hr at 30°C in presence of 5% (w/v) of each compound (Yan et al., 2014).

2.14 | Dynamic light scattering (DLS)

DLS experiments were conducted at 30°C using a Malvern Zetasizer Nano ZSP system. Translational diffusion coefficients (TDC) were obtained via measurements of the decay rates of scattered light and the autocorrelation curves. The hydrodynamic radius (H_R) of the *BaEstB* population was calculated from TDC on basis of the Stokes-Einstein equation assuming a spherical geometry of the molecules. Samples were centrifuged at 12,000g for 5 min before the measurements. Two set of experiments, (1) *BaEstB* without substrate and (2) *BaEstB* in presence of substrate (2-naphthyl acetate) were addressed; performing 12 scans for 10 s in both cases. DLS analysis of *BaEstB* with 2-naphthyl acetate was performed under the same conditions mentioned above considering its optimum pH and temperature. The data set replicates were analyzed using the DTS 5.10 software. Additionally, unfolding assays by temperature were performed in a range between 10 and 70°C. All measurements were performed in triplicate.

3 | RESULTS AND DISCUSSION

3.1 | Nucleotide sequence of *BaEstB*

A sequence with homology to the α/β hydrolase superfamily was identified from a cDNA library from *B. adusta* as described in materials and

methods. The cDNA sequence consisted of a 969 nucleotide (nt) ORF (GenBank accession number KX580963) and its genomic counterpart comprised 1,133 nt which contained three introns of 57, 50, and 57 nt, respectively (FS1 supplementary material). The first twenty-one hits of the PSI-Blast showed approximately 40%–49% identity and 87%–93% coverage that were annotated as fungal hypothetical proteins or α/β hydrolases (FS2 supplementary material). The 253th hit was the first with an assigned function showing 26% identity and 60% coverage with an esterase from *Acinetobacter* sp. (GeneBank BAB68337.1). Therefore, PSI-BLAST analysis suggests that this sequence belongs to the α/β hydrolase superfamily, however the majority of the proteins recovered from the PSI-BLAST are hypothetical or uncharacterized proteins and further studies are needed to assign its function. As a first approach to unravel *BaEstB* function, we decided to study its structure through bioinformatics analyses.

3.2 | *BaEstB* modeling

In the first attempt to model *BaEstB* (I-TASSER IDs: S243166 and S270524), the I-TASSER platform selected as templates esterases/lipases from the PDB [4WY8 and 4WY5 (*Rhizomucor miehei*), 4ZRS (esterase from metagenome), 4N5I and 4PO3 (*Lactobacillus rhamnosus*), 2O7R (*Actinidia eriantha*), and 3WJ1 (*Ferroplasma* sp.)]. We obtained a first three-dimensional model with TM-score of 0.75 ± 0.11 and C-score of 0.25. Being the PDB 4WY8 from a mucoral fungus and PDB 4ZRS the major templates, while other bacterial esterases/lipases and a plant carboxylesterase (PDB 2O7R from *Actinidia eriantha*) were also identified as templates by I-TASSER. The identification of the top 10 structural analogs in PDB always revealed proteins belonging to the HSL family (EC 3.1.1.79) (Table 1), this analysis strongly suggests that *BaEstB* is a member of this HSL family due to its structural similarity (Table 1, see TM-score, Coverage and RMSD values).

In order to obtain a more accurate three-dimensional model, we submitted a new modeling round (I-TASSER IDs: S248560 and S277038) using PDB 4ZRS and PDB 4WY8 as templates. The best model was obtained using PDB 4WY8 as template (Figure 1a) with a TM-score of 0.83 ± 0.10 and a C-score of 0.87. These score values confirm a high confidence in the quality of the model and additionally suggest the esterase/lipase activity of the *BaEstB*. The model obeyed to the canonical α/β -classical hydrolase architecture proposed by Ollis et al. (1992). During the second modeling, round I-TASSER identified as templates esterases belonging to the HSL family: PDB 4WY8 and 4WY5 (*Rhizomucor miehei*) and 3ZWQ (*Pyrobaculum calidifontis*). Again, HSL were the closest structural neighbors. The results above suggest that *BaEstB* belongs to HSL family.

Enzymes with lipolytic activity are classified into blocks C, L, H or X depending on their amino acid similarities and the presence of conserved motifs involved in the enzymatic catalysis (see ESTHER database) (Lenfant et al., 2013; Marchot & Chatonnet, 2012). Particularly, block H comprises two families: plant carboxylesterases and HSL, and its members are ubiquitous (see ESTHER database) (De Simone et al., 2004; Lenfant et al., 2013). According with this, it is not rare that PDB 2O7R was identified by I-TASSER as a template during the first

BaEstB modeling round, probably being *BaEstB* a member of block H. The HSL family is composed of esterases and lipases, and its members are widely represented in bacteria, plants, and animals (Tao et al., 2013). The HSL sequences identified in bacteria share high amino acid sequence similarity with the *LIPE* genes, which encode mammalian HSLs (Holm, 2003; Holm, Osterlund, Laurell, & Contreras, 2000). Two structural domains, cap and catalytic domains have been identified in HSL members, with the α/β -classical hydrolase fold (Yang,

Qin, et al., 2015). While several HSL have been structurally characterized in prokaryotic organisms (PDBs 2YH2, 1JJI, 3AIK, 1EVQ, 1JKM, etc.) (Dou et al., 2014; Ngo et al., 2013; Palm et al., 2011; Wei et al., 1999), only two HSL have been biochemically studied and crystallized in fungi (PDBs 4WY8 and 4WY5) (Yang, Qin, et al., 2015). 4WY8 and 4WY5 are the crystal structures of *RmEstB* and *RmEstA*, respectively, both esterases belonging to a member of the order Mucorales (Liu et al., 2013; Yan et al., 2014; Yang, Qin, et al., 2015). The structural

Rank	PDB	TM	RMSD	Cov.	Source	Family
1	4WY8	0.867	2.01	0.929	<i>Rhizomucor miehei</i>	HSL
2	4WY5	0.844	2.27	0.916	<i>Rhizomucor miehei</i>	HSL
3	4OU4	0.839	2.03	0.904	<i>Pseudomonas putida</i>	HSL
4	1JKM	0.836	2.24	0.910	<i>Bacillus subtilis</i>	HSL
5	4J7A	0.832	2.22	0.904	Metagenomic library	HSL
6	4N5I	0.831	2.43	0.907	<i>Lactobacillus rhamnosis</i>	Not available
7	3ZWQ	0.822	2.27	0.894	<i>Pyrobaculum calidifontis</i>	HSL
8	1LZL	0.820	2.20	0.894	<i>Rhodococcus</i> sp.	HSL
9	1JJI	0.814	2.07	0.879	<i>Archaeoglobus fulgidus</i>	HSL
10	1QZ3	0.811	2.29	0.891	<i>Alicyclobacillus acidocaldarius</i>	HSL

TABLE 1 Top 10 identified structural analogs in PDB

Ranking of proteins is based on TM-score of the structural alignment between the query structure and known structures in the PDB library.

TM: TM-score.

RMSD is the RMSD between residues that are structurally aligned by TM-align.

Cov.: Represents the coverage of the alignment by TM-align and is equal to the number of structurally aligned residues divided by length of the query protein.

HSL: Hormone-Sensitive Lipase.

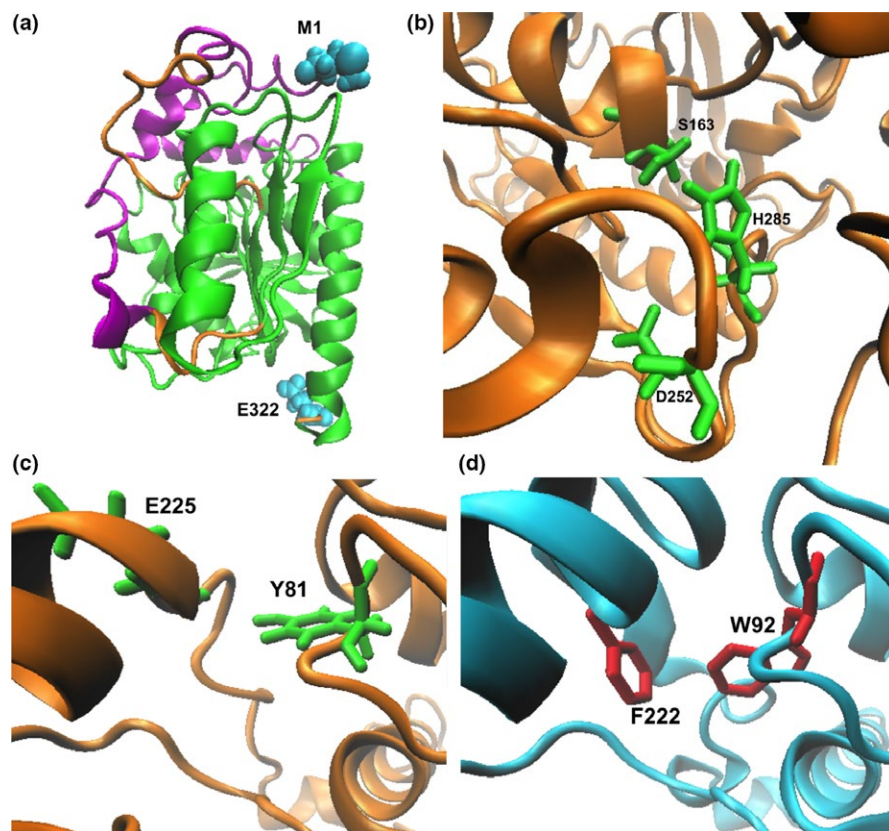


FIGURE 1 Structural analysis of *BaEstB*. (a) Three-dimensional model proposed for *BaEstB*. The cap and catalytic domains are depicted in magenta and green, respectively; while the N-terminal (M1) and C-terminal (E322) are shown in cyan. (b) Catalytic triad of *BaEstB*. S163, D252, and H285 are depicted in green. (c) and (d) Residues located in the center of the substrate-binding pocket. (c) Y81 and E225 are depicted in green in *BaEstB*, and (d) W92 and F222 are depicted in red in PDB 4WY8. All visualizations were performed in VMD

alignments with the previous fungal HSL allowed identifying the cap (purple) and the catalytic domains (green) in *BaEstB* (Figure 1a), as well as the catalytic triad, which was located in the respective canonical position. *BaEstB* cap domain comprises residues 1–39 and 209–238, while the catalytic domain includes residues 40–193 and 244–316 and shows the distinctive molecular topology described for other HSL: an α/β -hydrolase fold with a central β -sheet of eight mostly parallel strands surrounded by α -helices (Rozeboom, Godinho, Nardini, Quax, & Dijkstra, 2014; Yang, Qin, et al., 2015). The critical residues involved in the catalysis of *BaEstB* were identified in the following positions: S163, D252, and H285 (Figure 17b), being the canonical catalytic residues for HSL family. The three-dimensional superposition between PDB 4WY8 and *BaEstB* showed that the average RMSDs for the catalytic triad (S163, D252, and H285 in *BaEstB* vs. S164, D261, and H291 in PDB 4WY8) are 1.75, 5.28, and 4.68 Å, respectively.

Regarding the main structural characteristics of both, PDB 4WY8 and 4WY5, the critical residues located in the center of the substrate-binding pocket were identified in *BaEstB* also by structural alignments. *BaEstB* showed a higher similarity to *RmEstB* (4WY8) than to *RmEstA* (4WY5; see below). While two aromatic residues (W92 and F222) are found in *RmEstB*, an aromatic (Y81) and an acid residue (E225) are present in the centre of the *BaEstB*'s substrate-binding pocket (Figure 1c,d). The structural superposition allowed to calculate the average RMSDs for these residues between both proteins: 4.22 Å (W92 in PDB 4WY8 vs. Y81 in *BaEstB*) and 3.27 Å (F222 in PDB 4WY8 vs.

E225 in *BaEstB*). It is possible that these residues could be implicated in the narrowing of substrate range.

A three-dimensional superposition, considering the models derived from *RmEstB* (PDB 4WY8) and *BaEstB*, was prepared in VMD software previous a structural alignment of both models (Figure 2a). Values derived from the structural comparison such as TM-score of 0.925, Q_H -score of 0.849, and an overall RMSD of 0.9304 Å for 322 corresponding $C\alpha$ atoms, support a high structural homogeneity between both molecules (Figure 2a). The Q_H -score (metric value for structural alignment, $Q = 1$ when the proteins are identical), TM-score, and RMSD values are used to determine how good an alignment is between two proteins, and at the same time how similar they are structurally. The main differences of the molecular architectures were found in the loop regions, while the cap domain and the core of the enzymes exhibited a high structural superposition, showing a tertiary structure similarity (Figure 2b,c). These results confirm that *BaEstB* has the HSL canonical topology. Furthermore, superpositioning of *BaEstB* onto *RmEstB* revealed better overlay than the structural comparison between *RmEstA* and *RmEstB* according to the overall RMSD obtained for both analysis: 0.9304 versus 1.5117 Å, respectively. In this structural comparison, the Q_H value was also best for the *BaEstB*-*RmEstB* (0.849) superposition than that for *RmEstA*-*RmEstB* overlap (0.766). These data are interesting since *R. miehei* (Glomeromycota, subphylum Mucoromycotina) and *B. adusta* (Basidiomycota) are not phylogenetically close.

A structure-based phylogenetic tree constructed confirmed the results above according with the RMSD values derived from the

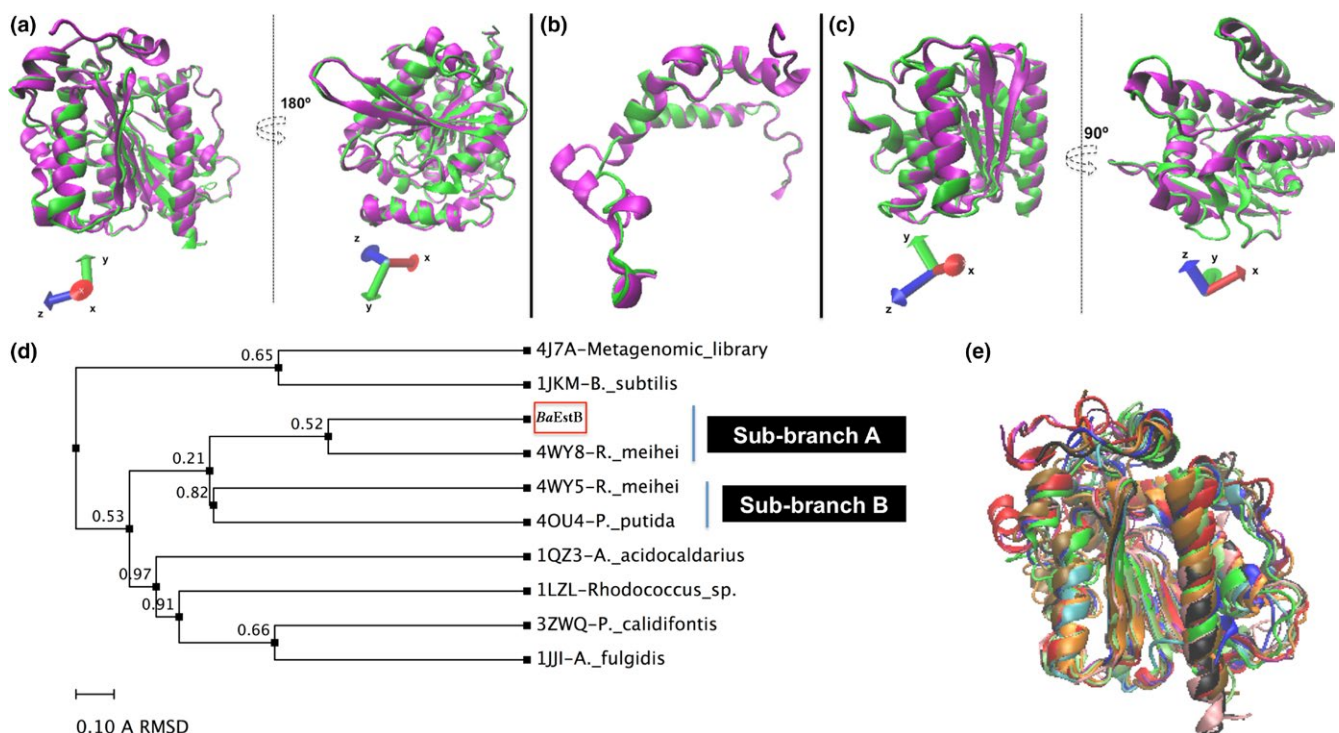


FIGURE 2 Superposition analysis between *RmEstB* (PDB 4WY8) and *BaEstB*. They are depicted in magenta and green, respectively. (a) Superpositioning of *BaEstB* onto *RmEstB* considering whole the sequence. (b) Superposition of cap domains. *RmEstB*: residues 3–51 and 206–247, and *BaEstB*: residues 1–39 and 209–238. (c) Superposition of catalytic domains. *RmEstB*: residues 52–191 and 253–322, and *BaEstB*: residues 40–193 and 244–322. (d) Structural-based phylogenetic trees constructed according to the RMSD derived from the *BaEstB*'s structural comparison with its closest structural analogs. (e) *BaEstB*'s superposition with its closest structural neighbors

BaEstB's structural comparison with its closest structural analogs (recovered by I-TASSER during our second modeling round) deposited in PDB (Figure 2d). This phylogenetic analysis showed that while *BaEstB* is grouped directly with *RmEstB* (PDB 4WY8) in the sub-branch A, *RmEstA* and *RmEstB* are resolved in different sub-branches (A and B), being *RmEstA* (PDB 4WY5) directly related with a *Pseudomonas putida*'s esterase (PDB 4OU4) grouped as sub-branch B (Figure 2d). These relations are supported by the average RMSD values obtained for both structural comparisons, and demonstrate that *RmEstB* is the characterized HSL microbial protein more phylogenetically related with *BaEstB*. Additionally, *BaEstB* was structurally overlaid with 10 PDB, recovered by I-TASSER, obtaining high structural similarity (Figure 2e). Superpositions Q_H values were between 0.6174 for PDB 1JKM and 0.849 for *RmEstB* as mentioned earlier, while RMSD values were up to 2.4934 Å. RMSD values of 2.4370, 2.4934, 2.1310, and 2.0931 Å were obtained for the topological comparison with PDB 4J7A, 1JKM, 1JJI, and 3ZWQ, respectively. These results are coherent with the distant phylogenetic relationship shown in Figure 2d. Overall, these data demonstrate that the basic architecture of HSL proteins is highly conserved in different microorganisms.

3.3 | Structural alignment analysis

Table 1 shows the nine crystallized HSL deposited in PDB that were used to perform the structural alignment, which were identified as its closest structural neighbors. The best alignment (17.10% of identity)

is shown with PDB 3ZWQ (*P. calidifontis*), while the lowest percentage identity (11.87%) was observed with a bacterial HSL homolog isolated from a metagenomic library (PDB 4J7A). The percentage identities between *BaEstB* vs. *RmEstA* and *RmEstB* were 15.63% and 16.91%, respectively (data not shown). Although the 10 sequences have low identity, they display a conserved molecular architecture. It has been reported in previous studies (Yang, Qin, et al., 2015) that cap domains are the worst alignment regions, however they share their tertiary structure as Figure 2b shows. Particularly, *BaEstB* does not exhibit sequence similarity in the cap domain with other HSL, not even with the fungal HSL (*RmEstA* and *RmEstB*).

From the alignment of the analyzed sequences, the HSL canonical catalytic triad (Ser-His-Asp) was located (Figure 3). In *BaEstB*, Ser163 is the nucleophile, His285 is the proton acceptor/donor, and Asp252 is the amino acid stabilizing His285. Additionally, the three signature motifs for HSL proteins were identified in *BaEstB*, and they were named as Block 1, 2, and 3 (Figure 3). The conserved tetrapeptide motif His-Gly-Gly-Gly (Block 1 in Figure 3) involved in the oxyanion cavity formation was identified in the aligned sequences and was located upstream of the active site. *BaEstB* sequence shows a conservative substitution in this motif (⁷⁷His-Gly-Gly-Ala⁸⁰), being this structural characteristic never reported for these proteins. It has been demonstrated that an Ala residue downstream of this signature motif is necessary to create the oxyanion cavity (Ngo et al., 2013; Yang, Qin, et al., 2015). We could find it in position 164 of *BaEstB*, being this amino acid extensively conserved in these sequences including the

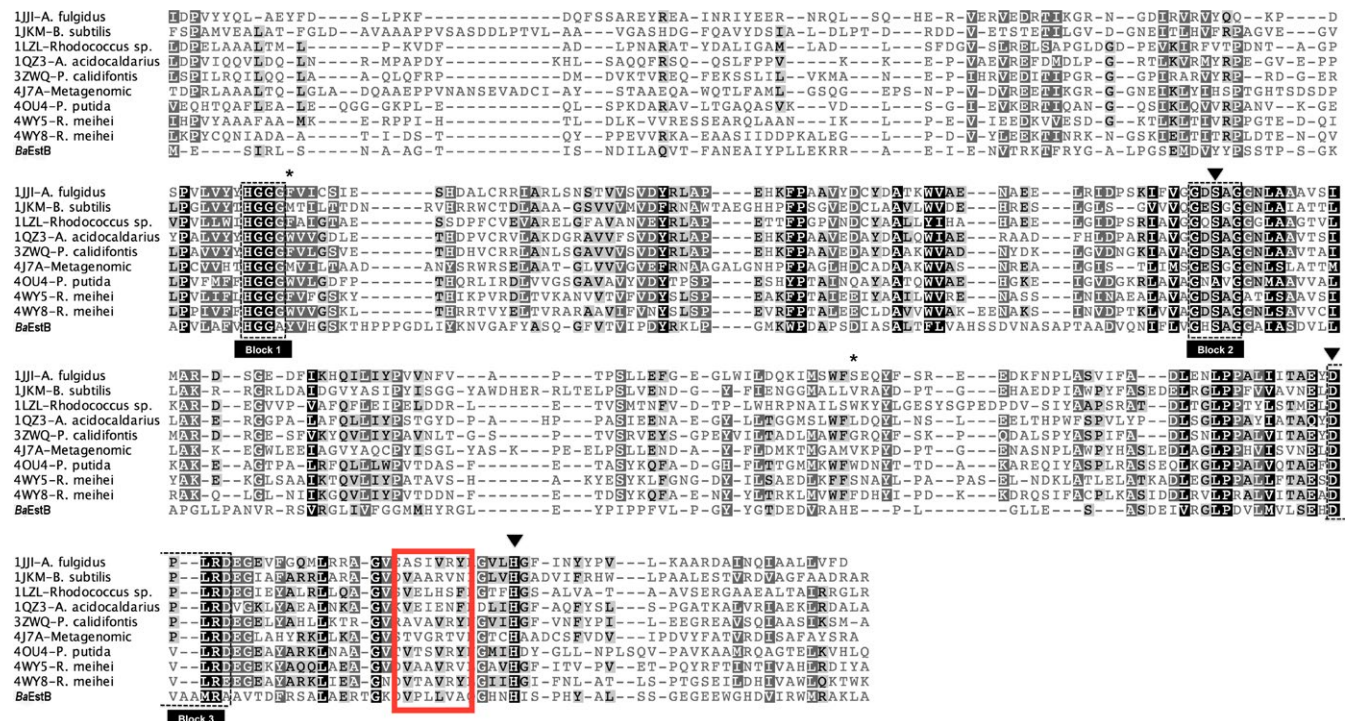


FIGURE 3 Structural alignment of *BaEstB* with HSL deposited in PDB: 4WY8, 4WY5, 4OU4, 1JKM, 4J7A, 3ZWQ, 1LZL, 1JJI and 1QZ3. The catalytic triad (Ser-His-Asp) is indicated with black triangles, while the amino acids located in the center of the substrate-binding pocket are marked with black asterisks. The alignment shows the typical domains in HSL esterases. Identical residues are shaded in black, and conserved residues are shaded in gray. The conserved catalytic motif is underlined. The three signature motifs for HSL proteins named Block 1, 2, and 3 are indicated as black dotted boxes. The putative catalytic nucleophile and acid/base are identified by a black filled arrow

Rhizomucor miehei's HLS (Ala163 and Ala165 in RmEst A and RmEstB, respectively); being Gly78, Gly79, and Ala164 the three amino acids involved in the oxyanion cavity formation in BaEstB.

On the other hand, the nucleophilic Ser163 is located in the characteristic ¹⁶⁰Gly-X-Ser-X-Gly¹⁶⁴ pentapeptide sequence (Block 2 in Figure 3). Some authors extend this block three more residues (Ngo et al., 2013), however these positions are less conserved in the block although it can define a consensus extended motif Gly-X-Ser-X-Gly-Gly-Asn-Leu. Gly and Leu being the most conserved and that are present in BaEstB: ¹⁶⁰Gly-X-Ser-X-Gly-Gly-Ala-Ile¹⁶⁷. A conservative change (Leu for Ile) and a nonconservative change (Asn for Ala) are present in BaEstB, while similar substitutions are found in the other sequences. A third conserved block Asp-Pro-X-X-Asp (Block 3 in Figure 3) involved in catalysis is common in HSL. BaEstB Block 3 is composed by ²⁵²Asp-Val-Ala-Ala-X-X-Ala²⁵⁸. The insertion of two Ala

residues, is a distinctive structural characteristic for BaEstB since in the other sequences it is not present. Moreover, in BaEstB and in both *R. miehei*'s HSL, a Pro residue is changed by Val. This substitution may be typical of fungi, since it is rarely found in bacteria (i.e., PDB 4OU4 of *P. putida*). Additionally, a nonconservative change is found in BaEstB, where an Asp is replaced by Ala. However, the positions X-X in the Asp-Pro-X-X-Asp motif is conserved (L and R) among all the sequences studied except in BaEstB (where we found M and R). Given this analysis, we cannot consider that the third block is conserved in BaEstB.

3.4 | Sequence phylogenetic analysis

The phylogenetic analysis based on the amino acid sequence showed that BaEstB is not grouped directly with any HSL member considered in the phylogeny reconstruction (Figure 4). This result is not

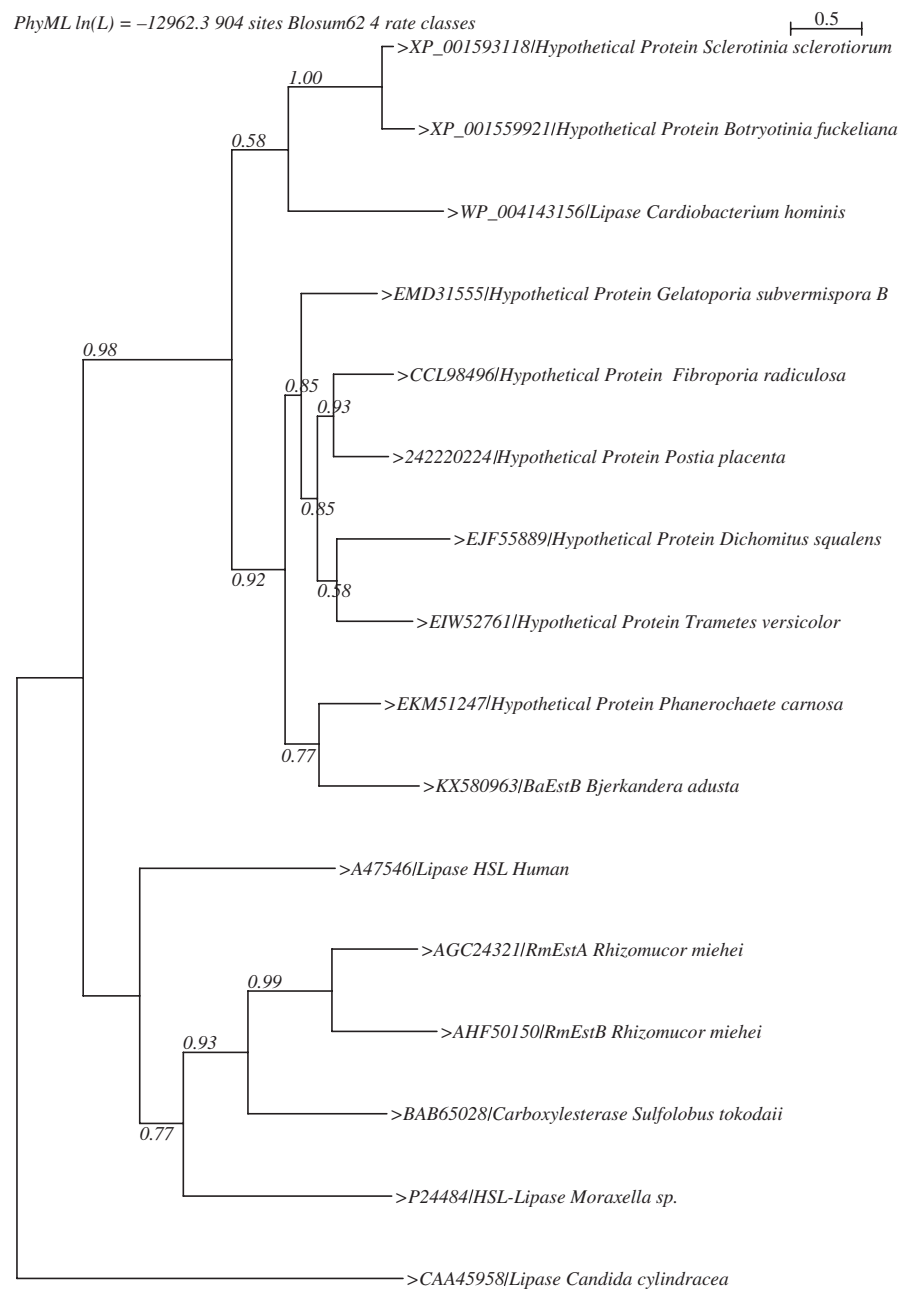


FIGURE 4 Phylogenetic reconstruction of BaEstB. The Maximum Likelihood method was used to estimate the phylogenetic tree; the branch support was assessed using the ALTr algorithm and the Jones-Thornton-Taylor (JTT) model was used to estimate distances for amino acids

surprising because *BaEstB* is a fungal protein with some distinctive structural characteristics as mentioned above. This relation could be supported by the low similarity coefficients observed in the multiple structural alignments. *BaEstB* is not directly related with *RmEstA* and *RmEstB*, which are also fungal proteins but from another distant Phylum (Glomeromycota, subphylum Mucoromycotina), which form a clade with bacterial HSL (Figure 4). The phylogeny suggests that these proteins presumably have a common ancestor since prokaryotic and fungal HSL share different clades. On the other hand, *BaEstB* groups with very good support values within a clade of hypothetical proteins all from Basidiomycetes. Taken together with the Blast results in which the first 21 hits showed identities of approximately 40%–49% (vs. 16.91% identity with *RmEstB* from *R. miehei*) and 87%–93% coverage (FS2 supplementary material), these results may suggest that the proteins in the first hits of the Blast could be HSL esterases in Basidiomycetes from the class Agaricomycetes.

3.5 | Expression and purification of *BaEstB* in *P. pastoris*

Oligonucleotides were designed to amplify the coding sequence of the putative esterase to be inserted in pJET, an intermediate vector. The cDNA was then subcloned in the expression vector pPICZ α A to be transformed in *P. pastoris* as has been described in material and methods section. Several independent colonies were induced with 0.5% methanol in BMMY medium and a qualitative assay using 2-naphthyl acetate was performed to select a colony that produced the best activity. *P. pastoris* wild type strain X-33 and a strain X-33 transformed with the empty vector showed no esterase activity. Three out of six

colonies were selected to perform a quantitative assay from culture supernatants. Strain *BaEstB5* was selected for further experiments. From this clone, *BaEstB* was purified through nickel affinity chromatography with 2.9-fold purification with recovery of 17% and specific activity of 31.58 U/mg using 2-naphthyl acetate (Table 2). The purified enzyme showed a single protein band both on SDS-PAGE and in a zymogram with an estimated molecular mass of 38.3 kDa (Figure 5a,b). The purified enzyme was used for its biochemical characterization.

3.6 | Biochemical characterization of *BaEstB*

3.6.1 | Substrate specificity

Since the α/β hydrolase family comprises both esterases and lipases, we performed a specific assay for lipases using rhodamine B together with commercial olive oil and monitoring the appearance of a fluorescent halo in ultra thin agar plates at λ 350 nm (Kouker & Jaeger, 1987). Concentrated supernatants of the wild type (wt) and a strain transformed with the empty vector or the purified *BaEstB* preparation did not show a fluorescent halo, contrary to a *Candida* lipase that was used as a positive control, showing that *BaEstB* has no lipase activity (data not shown).

In order to evaluate the substrate specificity of the enzyme, different *p*-NP esters with acyl chain lengths from C2 (*p*-NP acetate) to C16 (*p*-NP palmitate) were tested. Table 3 shows that enzyme activity declined along with longer chain-length, reaching 1.78 ± 0.33 U/mg with *p*-NP acetate (C2) and 0.99 ± 0.12 U/mg with *p*-NP butyrate (C4). Maximal hydrolytic activity was obtained against 2-naphthyl acetate with 31.58 ± 0.1 U/mg (C2) and no activity was detected against *p*-NP

TABLE 2 Results of the HSL purification from the heterologous expression system *P. pastoris*

	Volumetric activity (U/L)	Volume (ml)	Total units	Total protein	Specific activity (U/mg)	Purified fraction	Recuperation (%)
Supernatant- <i>BaEstB</i>	39.9	43	1.71	149.03	11	1	100
Pure <i>BaEstB</i>	193.15	1.5	0.29	15.2	31.58	2.9	17

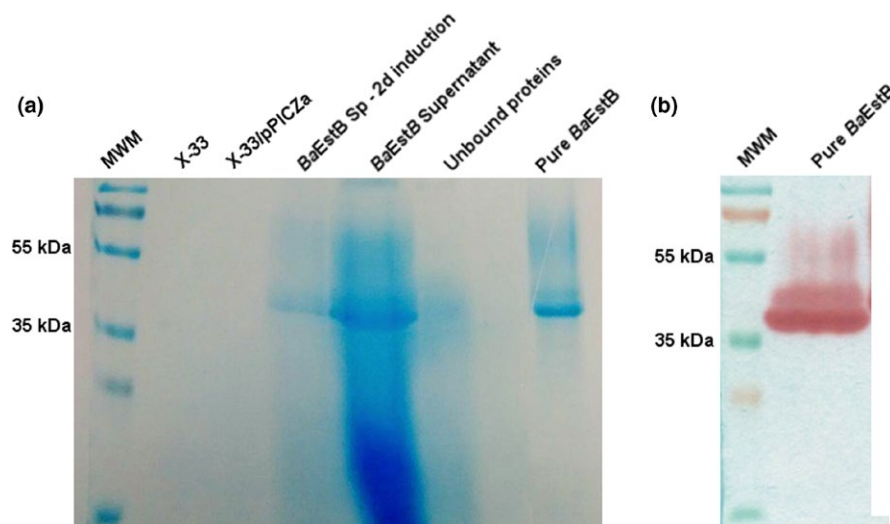


FIGURE 5 SDS-PAGE and zymogram analysis of the purified esterase from *B. adusta* (*BaEstB*). (a) Purification steps of *BaEstB* and (b) zymogram analysis of esterase on SDS-polyacrylamide gel using 2-naphthyl acetate as substrate

TABLE 3 Specific activity for of different substrates

Substrate	Specific activity ($\mu\text{mol}/\text{mg}$)
2-Naphthyl Acetate	31.58 ± 0.1
ρ -NP Acetate	1.78 ± 0.329
ρ -NP Butyrate	0.98 ± 0.115
ρ -NP Decanoate	0
ρ -NP Palmitate	0

esters with acyl chain lengths longer than C6. Together, these results indicated that the enzyme was an esterase with preference for short-chain esters. It is worth to note that the substrate specificity could be influenced by the size of the other moiety of the molecule, since 2-naphthyl acetate has two rings while ρ -NP esters have only one. If we compare the activity obtained with ρ -NP acetate versus that with 2-naphthyl acetate, an almost 18-fold difference is noted although the acyl chain is the same (acetate). This notion is supported by the fact that other esterases such as acetyl xylan esterases from family CE4, show a low activity on ρ -NP esters while they are very active on xylan, which is a polymer of xylopyranosyl residues. The difference on this activity is proposed to be due to the architecture of the neighboring sugars that allow the enzyme to better position itself in order to hydrolyze the acetate group (see Figure 12 in Biely, 2012) (Biely, 2012). As mentioned above, in mammals, HSL have bulky substrates such as cholesteryl esters. Taken together, these ideas suggest that *BaEstB* could be involved in unesterifying ergosterol esters, which have been detected by Yuan, Kuang, Wang, and Liu (2008) in different fungal tissues.

3.6.2 | Effect of temperature and pH on *BaEstB* activity

Optimal temperature and pH were determined for *BaEstB* over a temperature range from 10°C to 70°C and pH 4–11. This enzyme showed an optimal activity at 45°C (31.58 ± 0.1 U/mg), whereas at 30°C and

50°C still conserves 69% and 99% of activity, respectively. At lower temperatures, 20°C, it only shows 52% of the optimal activity and at 70°C it is almost inactivated. (Figure 6a). Thermostability of the enzyme was also determined. After incubation at different temperatures, we could determine that *BaEstB* conserves almost 81% of its activity after incubation at 40°C for 1 hr. Incubation at 10°C to 30°C showed around 97% of its activity, whereas incubation at 50°C abolished the activity to 5% (Figure 6b). HSL counterparts in *Rhizomucor* show similar optimal temperatures between 45 and 50°C (Liu et al., 2013; Yan et al., 2014), while other esterases from metagenomic libraries have their optimal temperatures around 30°C (Jeon et al., 2012; Li et al., 2014, 2015). Considering the temperature, *BaEstB* is a mesophilic HSL esterase, compared with a thermostable esterase from *Thermoanaerobacter tengcongensis* with optimal temperature at 70°C (Rao et al., 2011).

The purified *BaEstB* showed relatively high activity under alkaline conditions, and exhibited optimum activity at pH 7.0 in 50 mmol/L Tris-HCl (100%). The activity diminished only to 91% at pH 10; whereas at pH 11, the activity decreased to 53%. At the acidic pH 4, the enzyme has only 45% of activity (Figure 6c). We also determined the stability of the enzyme at different pH by incubating it in different buffers for 1 hr and then determining the activity. The most stable condition was found to be pH 7.0 showing 100% of activity, whereas at pH 6 the enzyme retained 69% of the activity. At more basic pH (from 8 to 10), the enzyme showed to be more stable since retained more than 90% of activity. However, at acidic pH 4, only around 20% residual activity was found (Figure 6d). As it was reported by Liu et al. (2013) for the *R. miehei* HSL enzymes, *BaEstB* also shows better activity in pHs around neutrality although it retains 50% of its activity even at pH 11. Compared with other HSL esterases, *BaEstB* retains its activity in a wider alkaline pH range. *BaEstB* optimal pH of 7.0 is lower than other esterases like that of an oil-degrading bacterium (pH 8.5) (Mizuguchi et al., 1999), *Pseudoalteromonas* sp (pH 8) (Cieśliński et al., 2007) or *Thermoanaerobacter tengcongensis* (pH 9.5) (Rao et al., 2011), but higher than an esterase from the basidiomycete *Pleurotus sapidus* (pH 6) (Linke et al., 2013).

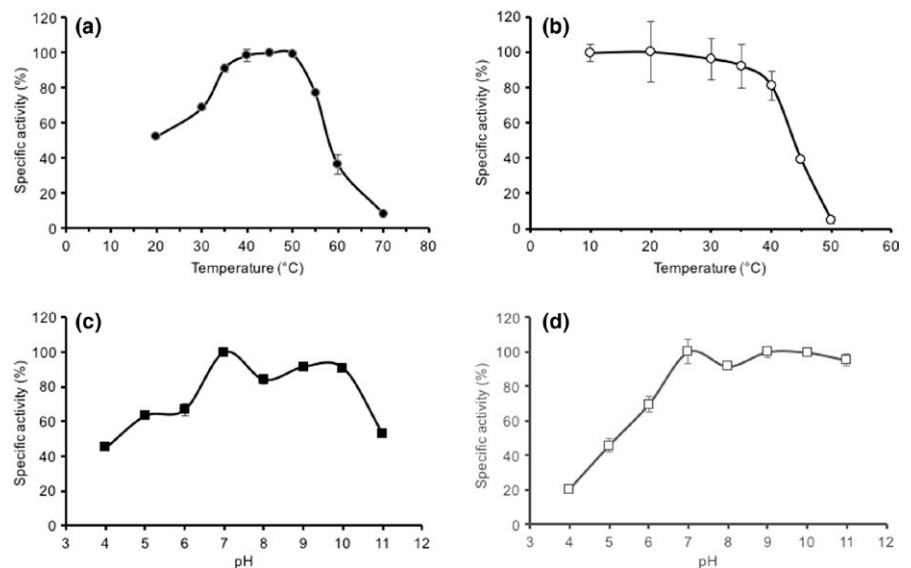


FIGURE 6 Effect of temperature and pH on the activity and stability of recombinant *BaEstB*. (a) Optimal temperature of *BaEstB* activity. (b) *BaEstB* thermal stability. (c) pH optimum for *BaEstB* activity and (d) pH stability for *BaEstB*

3.6.3 | *k*_{cat}, *K*_m, and ΔH determinations via ITC

The kinetic parameters of *BaEstB* were determined via ITC using its optimum pH and temperature. *BaEstB*'s kinetic properties were obtained plotting the "heat" values from the enzymatic reaction during 90 min (Figure 7a). The curve obtained from product formation velocity versus substrate concentration showed a high-quality adjustment via Michaelis–Menten equation ($\chi^2 = 1.153 \times 10^{-13}$) (Figure 7b), which is integrated in the used software. *BaEstB* showed a k_{catA} of $5.31 \times 10^3 \pm 20 \text{ s}^{-1}$ and K_{mA} of $7.68 \pm 0.62 \text{ }\mu\text{mol/L}$. The 2-naphthyl acetate hydrolysis is enthalpically favored by *BaEstB* ($\Delta H = -6.54 \times 10^4 \text{ cal/mol}$).

3.6.4 | Effects of metals, solvents, and detergents on *BaEstB* activity

The effects of various chemicals on the enzymatic activity were evaluated by measuring initial and residual activity after incubation (Table 4). The initial value is referred to that measured in a control

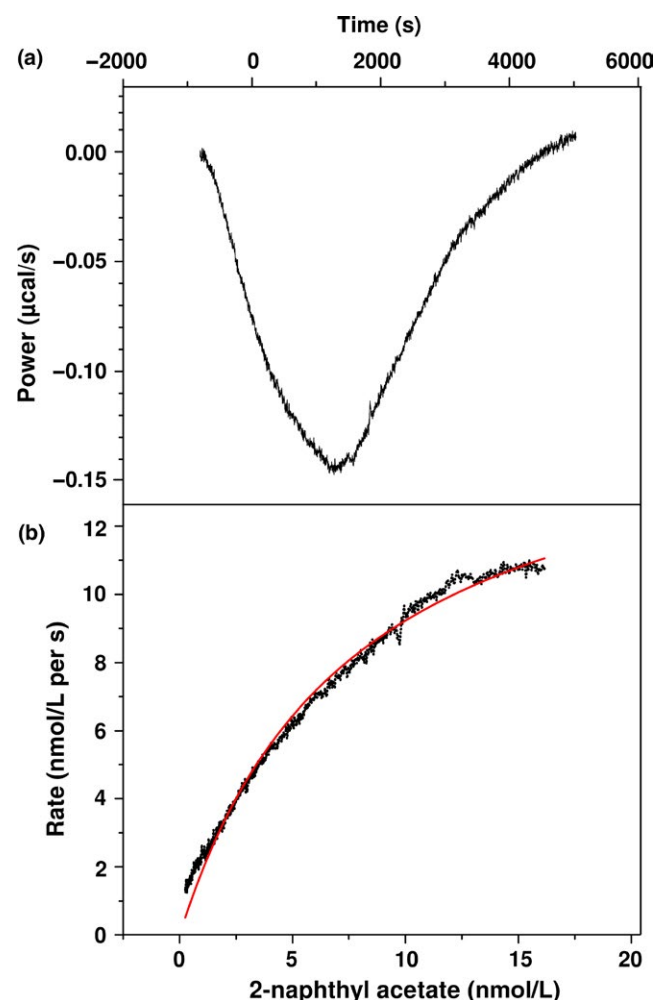


FIGURE 7 ITC analysis. (a) Curve plotting the "heat" values ($\mu\text{cal/s}$) from the enzymatic reaction during 5,400 s. (b) Curve obtained from product formation velocity (nmol/L per s) versus 2-naphthyl acetate concentration (nmol/L)

sample without the chemical, taken as 100% activity. Metal ions that slightly affected activity were Li^+ , K^+ , and Mg^{2+} . The *BaEstB* activity was strongly inhibited by Cu^{2+} (0.15%), Al^+ (0.68%), Fe^{2+} (0.78%), and Ag^{2+} (7%), and moderately inhibited by Mg^{2+} (74%), Li^+ (81.3%), and K^+ (75%). After an hour of incubation in the presence of these metals, the stability of the esterase is low. Also *BaEstB* shows slight halotolerance, at 0.1 mol/L NaCl the enzyme retained almost all its activity (91%) and it only diminished to 30% in the presence of 1 mol/L or

TABLE 4 Specific activity and residual activity in (%) of *BaEstB* with different divalent and monovalent ions and NaCl concentrations

Metal ions	Specific activity	Residual activity
No ions/No NaCl	100 \pm 1.63	44.57 \pm 1.78
Ba^{2+}	40.57 \pm 4.21	41.00 \pm 7.07
Mg^{2+}	73.64 \pm 1.02	25.61 \pm 3.11
Ca^{2+}	39.81 \pm 3.48	47.28 \pm 5.50
Mn^{2+}	28.82 \pm 3.72	17.31 \pm 4.84
Fe^{2+}	1.78 \pm 0.35	0.76 \pm 0.21
Co^{2+}	54.36 \pm 3.97	12.13 \pm 0.83
Ni^{2+}	15.53 \pm 2.92	0.29 \pm 0
Cu^{2+}	0.15 \pm 0.03	0.11 \pm 0.0001
Zn^{2+}	18.72 \pm 2.21	1.53 \pm 0.24
Ag^{2+}	6.88 \pm 0.91	4.19 \pm 0.88
K^+	74.64 \pm 8.73	33.8 \pm 3.22
Li^+	81.13 \pm 1.54	43.06 \pm 1.16
Al^+	0.68 \pm 0.16	0.13 \pm 0.03
NaCl concentration		
0.1 mol/L	91.29 \pm 9.53	61.72 \pm 0.78
0.25 mol/L	82.12 \pm 13.19	43.01 \pm 2.38
0.5 mol/L	69.42 \pm 10.11	43.00 \pm 0.80
1.0 mol/L	34.85 \pm 2.58	39.71 \pm 1.04
2.0 mol/L	30.99 \pm 4.36	39.43 \pm 1.74

Values represent the means of three replicates \pm standard error.

TABLE 5 Specific activity and residual activity in (%) of the *BaEstB* in the presence of solvents

Solvent	Specific activity	Residual activity
Not solvent	100 \pm 1.63	44.57 \pm 1.78
Ethanol	22.00 \pm 0.44	0.90 \pm 0.14
Methanol	6.18 \pm 1.23	8.45 \pm 1.01
Isopropanol	19.49 \pm 0.95	0.73 \pm 0.27
Butanol	49.48 \pm 4.14	0.35 \pm 0.10
Acetone	7.33 \pm 0.37	0.49 \pm 0.09
Acetonitrile	3.55 \pm 0.74	0.29 \pm 0.41
Chloroform	82.79 \pm 6.04	16.98 \pm 3.09
Hexane	40.14 \pm 4.55	64.77 \pm 4.32
DMSO	13.10 \pm 1.55	36.11 \pm 3.25

Values represent the means of three replicates \pm standard error.

TABLE 6 Specific activity and residual activity in (%) of *BaEstB* in the presence of detergents

Detergent	Specific activity	Residual activity
Not detergent	100 ± 1.63	44.57 ± 1.78
Tween 20	0.27 ± 0.08	0.74 ± 0.34
Tween 80	0.69 ± 0.17	1.55 ± 0.54
Triton X-100	16.14 ± 3.79	43.47 ± 0.96
SDS	0.33 ± 0.06	0.49 ± 0.34
CTAB	2.22 ± 0.37	1.10 ± 0.44
EDTA	29.91 ± 7.37	51.03 ± 4.67

2 mol/L NaCl indicating a slight tolerance to salinity. In contrast, an esterase isolated from a metagenomic library has a high halotolerance showing more activity in presence of salt (Selvin et al., 2012).

The enzyme activity of *BaEstB* was significantly inactivated in the presence of methanol, isopropanol, ethanol, acetone, DMSO, and hexane. In the presence of 1-butanol and chloroform, the reduction was not as severe, showing 50% and 82%, respectively (Table 5). However, in all the cases, the residual activity was low. Furthermore, the enzyme's activity was significantly abolished in the presence of different detergents such as Tween 20, Tween 80, Triton X-100, SDS and CTAB, as well as a chelant agent, EDTA (Table 6).

3.6.5 | DLS analysis

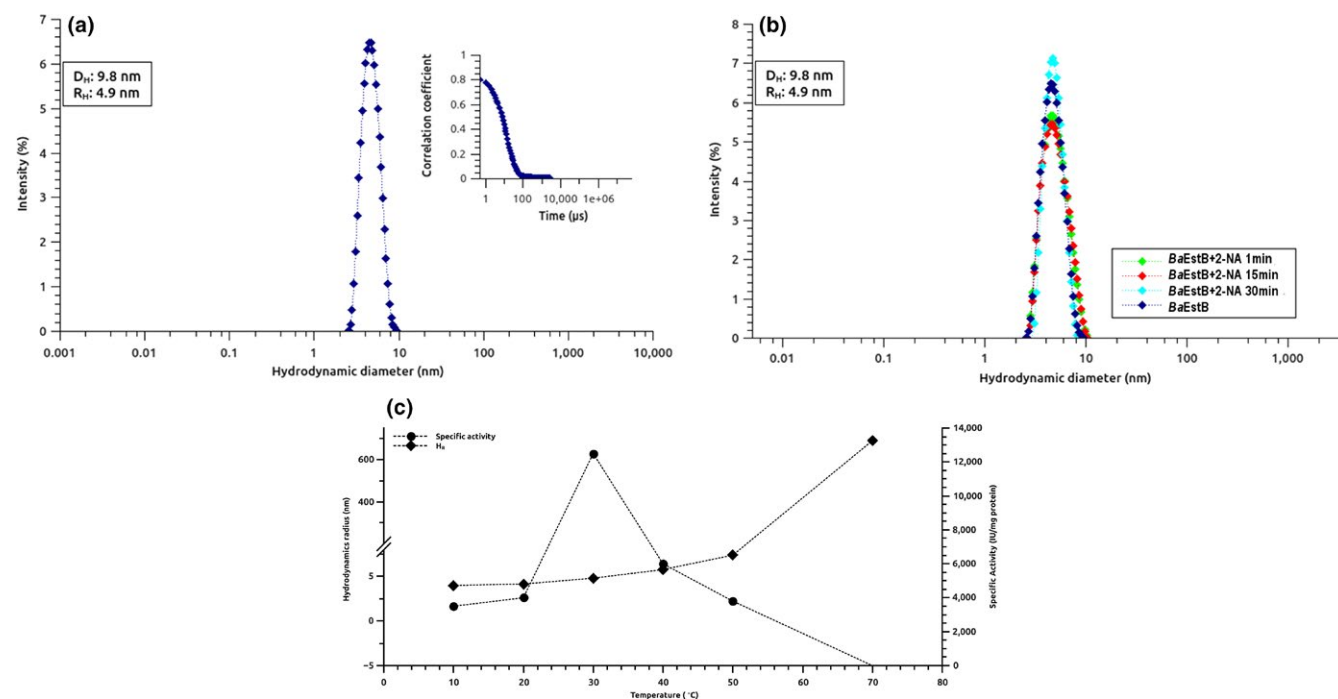
Figure 8a depicts the light scattering intensity (%) versus the hydrodynamic diameter (nm), showing a single *BaEstB* population with a H_R

of 4.9 nm. This value suggests a dimeric state for *BaEstB* according to the expected H_R (5.4 nm) for a protein of 38.3 kDa (monomeric state). The correlation curve (Figure 8a, upper) supports the high quality of DLS analysis. A second experiment with *BaEstB* preparations in the presence of 2-naphthyl acetate was performed in order to demonstrate any effect of the substrate on the oligomeric state of the enzyme. Figure 8b suggests that the dimeric conformation of *BaEstB* is maintained during its interaction with the substrate (the same H_R value was obtained).

Figure 8c shows the relationship between hydrodynamic radius and temperature. Hydrodynamic radius values increase while temperature is higher, indicating the unfolding of *BaEstB*. The hydrodynamic radius at 70°C suggests that *BaEstB* is totally unfolding and it is in correspondence with its specific activity at this temperature (0 IU/mg protein). Other HSL enzymes, as PDB 4J7A isolated from a metagenome (Ngo et al., 2013) and PDB 4WY5 from *R. miehei* (Yang, Qin, et al., 2015), have been also reported as dimers, the latter forming a tetrameric structure through hydrogen bonding; supporting our results that show that *BaEstB* is constituted as a dimer.

CONCLUSIONS

In this work, we report for the first time a HSL from a Basidiomycete fungus. The genomic sequence contains three small introns which is not unusual for Basidiomycetes. Through three-dimensional modeling studies and phylogenetic analysis, we conclude that *BaEstB* is an ortholog of the previously described *RmEstB* HSL of *R. miehei*. Traditional phylogenetic analysis together with Blastx results,

**FIGURE 8** DLS analysis. (a) Hydrodynamic diameter determination of *BaEstB* population without substrate. (b) Hydrodynamic diameter determination of *BaEstB* population in presence of 2-naphthyl acetate. (c) Relationship between hydrodynamic radius and temperature

suggests that a number of fungal hypothetical proteins could belong to the HSL family.

ACKNOWLEDGMENTS

We are grateful to Dr. Agustín López Munguía for providing bench space at his laboratory and to Rocío Rodríguez-Hernández for contributing with experimental material. We feel thankful to Jorge Yáñez, Santiago Becerra, Paul Gaytán, Eugenio López for synthesis of DNA and DNA sequencing. Part of the research was performed at the LabDP-UAEM.

CONFLICT OF INTEREST

The authors declare that they have no conflicts of interest with the contents of this article.

REFERENCES

- Akoh, C. C., Lee, G.-C., Liaw, Y.-C., Huang, T.-H., & Shaw, J.-F. (2004). GDSL family of serine esterases/lipases. *Progress in Lipid Research*, 43, 534–552.
- Ali, Y. B., Verger, R., & Abousalham, A. (2012). Lipases or esterases: Does it really matter? Toward a new bio-physico-chemical classification. *Methods in Molecular Biology (Clifton NJ)*, 861, 31–51.
- Andualema, B., & Gessesse, A. (2012). Microbial lipases and their industrial applications: Review. *Biotechnology*, 11, 100–118.
- Anobom, C. D., Pinheiro, A. S., De-Andrade, R. A., Agueiras, E. C. G., Andrade, G. C., Moura, M. V., ... Freire, D. M. (2014). From structure to catalysis: Recent developments in the biotechnological applications of lipases. *BioMed Research International*, 2014, 684506.
- Arpigny, J. L., & Jaeger, K. E. (1999). Bacterial lipolytic enzymes: Classification and properties. *Biochemical Journal*, 343(Pt 1), 177–183.
- Bancerz, R., & Ginalska, G. (2007). A novel thermostable lipase from basidiomycete *Bjerkandera adusta* R59: Characterisation and esterification studies. *Journal of Industrial Microbiology and Biotechnology*, 34, 553–560.
- Barriuso, J., Prieto, A., & Martínez, M. J. (2013). Fungal genomes mining to discover novel sterol esterases and lipases as catalysts. *BMC Genomics*, 14, 712.
- Belcarz, A., Ginalska, G., & Kornilowicz-Kowalska, T. (2005). Extracellular enzyme activities of *Bjerkandera adusta* R59 soil strain, capable of daunomycin and humic acids degradation. *Applied Microbiology and Biotechnology*, 68, 686–694.
- Biely, P. (2012). Microbial carbohydrate esterases deacetylating plant polysaccharides. *Biotechnology Advances*, 30, 1575–1588.
- Bornscheuer, U. T. (2002). Microbial carboxyl esterases: Classification, properties and application in biocatalysis. *FEMS Microbiology Reviews*, 26, 73–81.
- Borrelli, G. M., & Trono, D. (2015). Recombinant lipases and phospholipases and their use as biocatalysts for industrial applications. *International Journal of Molecular Sciences*, 16, 20774–20840.
- Carrière, F., Withers-Martinez, C., van Tilbeurgh, H., Roussel, A., Cambillau, C., & Verger, R. (1998). Structural basis for the substrate selectivity of pancreatic lipases and some related proteins. *Biochimica et Biophysica Acta*, 1376, 417–432.
- Chahinian, H., & Sarda, L. (2009). Distinction between esterases and lipases: Comparative biochemical properties of sequence-related carboxylesterases. *Protein and Peptide Letters*, 16, 1149–1161.
- Ciesliński, H., Białkowska, A. M., Długotecka, A., Daroch, M., Tkaczuk, K. L., Kalinowska, H., ... Turkiewicz, M. (2007). A cold-adapted esterase from psychrotrophic *Pseudoalteromas* sp. strain 643A. *Archives of Microbiology*, 188, 27–36.
- Cuervo-Soto, L. I., Valdés-García, G., Batista-García, R., Del Rayo Sánchez-Carbente M., Balcázar-López, E., Lira-Ruan, V., ... Folch-Mallol, J. L. (2015). Identification of a novel carbohydrate esterase from *Bjerkandera adusta*: Structural and function predictions through bioinformatics analysis and molecular modeling. *Proteins*, 83, 533–546.
- De Simone, G., Mandrich, L., Menchise, V., Giordano, V., Febbraio, F., Rossi, M., ... Manco, G. (2004). A substrate-induced switch in the reaction mechanism of a thermophilic esterase: Kinetic evidences and structural basis. *Journal of Biological Chemistry*, 279, 6815–6823.
- Dereeper, A., Audic, S., Claverie, J.-M., & Blanc, G. (2010). BLAST-EXPLORER helps you building datasets for phylogenetic analysis. *BMC Evolutionary Biology*, 10, 8.
- Dereeper, A., Guignon, V., Blanc, G., Audic, S., Buffet, S., Chevenet, F., ... Gascuel, O. (2008). Phylogeny.fr: Robust phylogenetic analysis for the non-specialist. *Nucleic Acids Research*, 36, W465–W469.
- Dou, S., Kong, X.-D., Ma, B.-D., Chen, Q., Zhang, J., Zhou, J., & Xu, J.-H. (2014). Crystal structures of *Pseudomonas putida* esterase reveal the functional role of residues 187 and 287 in substrate binding and chiral recognition. *Biochemical and Biophysical Research Communications*, 446, 1145–1150.
- Fojan, P., Jonson, P. H., Petersen, M. T., & Petersen, S. B. (2000). What distinguishes an esterase from a lipase: A novel structural approach. *Biochimie*, 82, 1033–1041.
- Gopinath, S. C. B., Anbu, P., Lakshmi Priya, T., & Hilda, A. (2013). Strategies to characterize fungal lipases for applications in medicine and dairy industry. *BioMed Research International*, 2013, 154549.
- Holick, M. F. (2003). Vitamin D: A millenium perspective. *Journal of Cellular Biochemistry*, 88, 296–307.
- Holm, C. (2003). Molecular mechanisms regulating hormone-sensitive lipase and lipolysis. *Biochemical Society Transactions*, 31, 1120–1124.
- Holm, C., Osterlund, T., Laurell, H., & Contreras, J. A. (2000). Molecular mechanisms regulating hormone-sensitive lipase and lipolysis. *Annual Review of Nutrition*, 20, 365–393.
- Houde, A., Kademi, A., & Leblanc, D. (2004). Lipases and their industrial applications: An overview. *Applied Biochemistry and Biotechnology*, 118, 155–170.
- Huang, J., Huo, Y.-Y., Ji, R., Kuang, S., Ji, C., Xu, X.-W., & Li, J. (2016). Structural insights of a hormone sensitive lipase homologue Est22. *Scientific Reports*, 6, 28550.
- Humphrey, W., Dalke, A., & Schulten, K. (1996). VMD: Visual molecular dynamics. *Journal of Molecular Graphics*, 14(33–38), 27–28.
- Jaeger, K. E., Dijkstra, B. W., & Reetz, M. T. (1999). Bacterial biocatalysts: Molecular biology, three-dimensional structures, and biotechnological applications of lipases. *Annual Review of Microbiology*, 53, 315–351.
- Jeon, J. H., Lee, H. S., Kim, J. T., Kim, S.-J., Choi, S. H., Kang, S. G., & Lee, J.-H. (2012). Identification of a new subfamily of salt-tolerant esterases from a metagenomic library of tidal flat sediment. *Applied Microbiology and Biotechnology*, 93, 623–631.
- Karpushova, A., Brümmer, F., Barth, S., Lange, S., & Schmid, R. D. (2005). Cloning, recombinant expression and biochemical characterisation of novel esterases from *Bacillus* sp. associated with the marine sponge *Aplysina aerophoba*. *Applied Microbiology and Biotechnology*, 67, 59–69.
- Kouker, G., & Jaeger, K. E. (1987). Specific and sensitive plate assay for bacterial lipases. *Applied and Environment Microbiology*, 53, 211–213.
- Kraemer, F. B. (2007). Adrenal cholesterol utilization. *Molecular and Cellular Endocrinology*, 265–266, 42–45.
- Laemmli, U. K. (1970). Cleavage of structural proteins during the assembly of the head of bacteriophage T4. *Nature*, 227, 680–685.
- Lenfant, N., Hotelier, T., Velluet, E., Bourne, Y., Marchot, P., & Chatonnet, A. (2013). ESTHER, the database of the α/β -hydrolase fold superfamily of proteins: Tools to explore diversity of functions. *Nucleic Acids Research*, 41, D423–D429.

- Li, P.-Y., Chen, X.-L., Ji, P., Li, C.-Y., Wang, P., Zhang, Y., ... Zhang, X.-Y. (2015). Interdomain hydrophobic interactions modulate the thermostability of microbial esterases from the hormone-sensitive lipase family. *Journal of Biological Chemistry*, 290, 11188–11198.
- Li, P.-Y., Ji, P., Li, C.-Y., Zhang, Y., Wang, G.-L., Zhang, X.-Y., ... Zhang, Y.-Z. (2014). Structural basis for dimerization and catalysis of a novel esterase from the GTSAG motif subfamily of the bacterial hormone-sensitive lipase family. *Journal of Biological Chemistry*, 289, 19031–19041.
- Linke, D., Matthes, R., Nimtz, M., Zorn, H., Bunzel, M., & Berger, R. G. (2013). An esterase from the basidiomycete *Pleurotus sapidus* hydrolyzes feruloylated saccharides. *Applied Microbiology and Biotechnology*, 97, 7241–7251.
- Liu, Y., Xu, H., Yan, Q., Yang, S., Duan, X., & Jiang, Z. (2013). Biochemical characterization of a first fungal esterase from *Rhizomucor miehei* showing high efficiency of ester synthesis. *PLoS ONE*, 8, e77856.
- Lopes, D. B., Fraga, L. P., Fleuri, L. F., & Macedo, G. A. (2011). Lipase and esterase: To what extent can this classification be applied accurately? *Food Sci Technol Camp*, 31, 603–613.
- Marchot, P., & Chatonnet, A. (2012). Enzymatic activity and protein interactions in alpha/beta hydrolase fold proteins: Moonlighting versus promiscuity. *Protein and Peptide Letters*, 19, 132–143.
- Mizuguchi, S., Amada, K., Haruki, M., Imanaka, T., Morikawa, M., & Kanaya, S. (1999). Identification of the gene encoding esterase, a homolog of hormone-sensitive lipase, from an oil-degrading bacterium, strain HD-1. *J Biochem (Tokyo)*, 126, 731–737.
- Ngo, T. D., Ryu, B. H., Ju, H., Jang, E., Park, K., Kim, K. K., & Kim, T. D. (2013). Structural and functional analyses of a bacterial homologue of hormone-sensitive lipase from a metagenomic library. *Acta Crystallographica. Section D, Biological Crystallography*, 69, 1726–1737.
- Ollis, D. L., Cheah, E., Cygler, M., Dijkstra, B., Frolow, F., Franken, S. M., ... Schrag, J. (1992). The alpha/beta hydrolase fold. *Protein Engineering*, 5, 197–211.
- Palm, G. J., Fernández-Álvarez, E., Bogdanović, X., Bartsch, S., Sczodrok, J., Singh, R. K., ... Hinrichs, W. (2011). The crystal structure of an esterase from the hyperthermophilic microorganism *Pyrobaculum calidifontis* VA1 explains its enantioselectivity. *Applied Microbiology and Biotechnology*, 91, 1061–1072.
- Quiroz-Castañeda, R. E., Balcázar-López, E., Dantán-González, E., Martínez, A., Folch-Mallol, J., & Martínez Anaya, C. (2009). Characterization of cellulolytic activities of *Bjerkandera adusta* and *Pycnoporus sanguineus* on solid wheat straw medium. *Electronic Journal of Biotechnology*, 12, 5–6.
- Quiroz-Castañeda, R. E., Martínez-Anaya, C., Cuervo-Soto, L. I., Segovia, L., & Folch-Mallol, J. L. (2011). Loosenin, a novel protein with cellulose-disrupting activity from *Bjerkandera adusta*. *Microb Cell Factories*, 10, 8.
- Quiroz-Castañeda, R. E., Pérez-Mejía, N., Martínez-Anaya, C., Acosta-Urdapilleta, L., & Folch-Mallol, J. (2011). Evaluation of different lignocellulosic substrates for the production of cellulases and xylanases by the basidiomycete fungi *Bjerkandera adusta* and *Pycnoporus sanguineus*. *Biodegradation*, 22, 565–572.
- Rao, L., Xue, Y., Zhou, C., Tao, J., Li, G., Lu, J. R., & Ma, Y. (2011). A thermostable esterase from *Thermoanaerobacter tengcongensis* opening up a new family of bacterial lipolytic enzymes. *Biochimica et Biophysica Acta*, 1814, 1695–1702.
- Romero, E., Speranza, M., García-Guinea, J., Martínez, A. T., & Martínez, M. J. (2007). An anamorph of the white-rot fungus *Bjerkandera adusta* capable of colonizing and degrading compact disc components. *FEMS Microbiology Letters*, 275, 122–129.
- Roy, A., Kucukural, A., & Zhang, Y. (2010). I-TASSER: A unified platform for automated protein structure and function prediction. *Nature Protocols*, 5, 725–738.
- Rozeboom, H. J., Godinho, L. F., Nardini, M., Quax, W. J., & Dijkstra, B. W. (2014). Crystal structures of two *Bacillus* carboxylesterases with different enantioselectivities. *Biochimica et Biophysica Acta*, 1844, 567–575.
- Selvin, J., Kennedy, J., Lejon, D. P., Kiran, G. S., & Dobson, A. D. (2012). Isolation identification and biochemical characterization of a novel halo-tolerant lipase from the metagenome of the marine sponge *Haliclona simulans*. *Microb Cell Factories*, 11, 72.
- Shobayashi, M., Mitsueda, S., Ago, M., Fujii, T., Iwashita, K., & Iefuji, H. (2005). Effects of culture conditions on ergosterol biosynthesis by *Saccharomyces cerevisiae*. *Bioscience, Biotechnology, and Biochemistry*, 69, 2381–2388.
- Soberanes Céspedes, N., Cruz, R. R., Vargas, M. S., & Vázquez, Z. G. (2012). Variabilidad en la actividad general de esterases de la garrapata *Boophilus microplus* y su relación con la resistencia a organofosforados. *Rev Mex Cienc Pecu*, 43, 239–246.
- Sun, S., Gao, Y., Ling, X., & Lou, H. (2005). The combination effects of phenolic compounds and fluconazole on the formation of ergosterol in *Candida albicans* determined by high-performance liquid chromatography/tandem mass spectrometry. *Analytical Biochemistry*, 336, 39–45.
- Tao, W., Shengxue, F., Duobin, M., Xuan, Y., Congcong, D., & Xihua, W. (2013). Characterization of a new thermophilic and acid tolerant esterase from *Thermotoga maritima* capable of hydrolytic resolution of racemic ketoprofen ethyl ester. *Journal of Molecular Catalysis. B, Enzymatic*, 85–86, 23–30.
- Wang, Y., Vazquez-Duhalt, R., & Pickard, M. A. (2003). Manganese-lignin peroxidase hybrid from *Bjerkandera adusta* oxidizes polycyclic aromatic hydrocarbons more actively in the absence of manganese. *Canadian Journal of Microbiology*, 49, 675–682.
- Wei, Y., Contreras, J. A., Sheffield, P., Osterlund, T., Derewenda, U., Kneusel, R. E., ... Derewenda, Z. S. (1999). Crystal structure of brefeldin A esterase, a bacterial homolog of the mammalian hormone-sensitive lipase. *Natural Structural Biology*, 6, 340–345.
- Yan, Q., Yang, S., Duan, X., Xu, H., Liu, Y., & Jiang, Z. (2014). Characterization of a novel hormone-sensitive lipase family esterase from *Rhizomucor miehei* with tertiary alcohol hydrolysis activity. *Journal of Molecular Catalysis. B, Enzymatic*, 109, 76–84.
- Yang, S., Qin, Z., Duan, X., Yan, Q., & Jiang, Z. (2015). Structural insights into the substrate specificity of two esterases from the thermophilic *Rhizomucor miehei*. *Journal of Lipid Research*, 56, 1616–1624.
- Yang, J., Yan, R., Roy, A., Xu, D., Poisson, J., & Zhang, Y. (2015). The I-TASSER Suite: Protein structure and function prediction. *Nature Methods*, 12, 7–8.
- Yuan, J.-P., Kuang, H.-C., Wang, J.-H., & Liu, X. (2008). Evaluation of ergosterol and its esters in the pileus, gill, and stipe tissues of agaric fungi and their relative changes in the comminuted fungal tissues. *Applied Microbiology and Biotechnology*, 80, 459–465.
- Zhang, Y. (2008). I-TASSER server for protein 3D structure prediction. *BMC Bioinformatics*, 9, 40.
- Zweytick, D., Athenstaedt, K., & Daum, G. (2000). Intracellular lipid particles of eukaryotic cells. *Biochimica et Biophysica Acta*, 1469, 101–120.

SUPPORTING INFORMATION

Additional Supporting Information may be found online in the supporting information tab for this article.

How to cite this article: Sánchez-Carbente MR, Batista-García RA, Sánchez-Reyes A, et al. The first description of a hormone-sensitive lipase from a basidiomycete: Structural insights and biochemical characterization revealed *Bjerkandera adusta* BaEstB as a novel esterase. *MicrobiologyOpen*. 2017;6:e463. <https://doi.org/10.1002/mbo3.463>